

## Provenance tracing of long-range transported dust over the Northeastern Arabian Sea during the southwest monsoon

Suresh K.<sup>1,2</sup>, Udisha Singh<sup>1,3</sup>, Ashwini Kumar<sup>1\*</sup>, Damodararao Karri<sup>1</sup>, Aditya Peketi<sup>1</sup>, V. Ramaswamy<sup>1</sup>

<sup>1</sup>CSIR-National Institute of Oceanography, Dona Paula, Goa, India

<sup>2</sup>School of Earth, Ocean and Atmospheric Sciences, Goa University, Goa, India

<sup>3</sup>Academy of Scientific and Innovative Research (AcSIR), CSIR-National Institute of Oceanography, Goa, India

\*Corresponding author:

Ashwini Kumar

Geological Oceanography Division

CSIR-National Institute of Oceanography

Dona Paula, Goa-403 004

E-mail: ashwinikumarjha@gmail.com,

ashwinik@nio.org

Tel: +91 832 2450368, Fax: +91 832 2450602

### Abstract

One of the major pathways for dust supply to surface water of the Arabian Sea is via wet deposition, which is significant during southwest Monsoon (June-September). Aeolian dust supplies macro and micronutrients, which can impact on several marine biogeochemical processes. Here we report, major elements and rare earth elements (REEs) content as well as mineralogical and Sr-Nd isotopic composition of particulate collected from wet deposition (WDP) during the southwest monsoon period over the Northeastern Arabian Sea (NEAS) (Goa; 15.4° N, 73.8° E) in 2013. The collected WDP samples are classified into three categories based on changing wind regime, namely: (1) beginning of monsoon (BM; June); (2) mid of monsoon (MM; July-August) and (3) end of monsoon (EM; September). Our result highlights a significant temporal variability in REEs pattern showing a decreasing trend of  $L_n/Y_n$  and relatively higher  $Eu^*/Eu$  anomaly during mid of monsoon compared to beginning and end of monsoon period. High palygorskite (P) with moderate smectite (S) is observed for beginning of monsoon and majority of mid monsoon samples, however, high smectite with moderate palygorskite and negligible palygorskite and smectite abundance is observed for few of mid monsoon and end of monsoon samples, respectively, indicating change in dust sources during the southwest monsoon period. We also observed temporal variability in  $^{87}Sr/^{86}Sr$  (0.7090-0.7193) and  $\epsilon_{Nd}$  (-2.3 to -9.1) isotopic compositions wherein less radiogenic  $^{87}Sr/^{86}Sr$  and relatively more positive  $\epsilon_{Nd}$  is exhibited by mid of monsoon samples compared to those observed in beginning and end of monsoon collections. The seasonal variability in geochemical tracers are related to changes in the dust source areas which are identified as (1) the Arabian Peninsula contributing significantly in beginning of monsoon and majority of mid monsoon samples; (2) Northeastern Africa contributing to some of the mid monsoon samples and (3) Southwest Asia and Thar Desert in end of monsoon samples. These source identification using geochemical tracers are corroborated by the satellite images (CALIPSO and aerosol index maps) and back-trajectory analyses.

**Keywords:** Arabian Sea, Mineral dust, Sr-Nd isotopes, Clay mineralogy, Wet deposition.

## 1. Introduction

Long-range transport of atmospheric mineral dust and their deposition supplies essential macro and micro-nutrients to continental as well as ocean ecosystem (Prospero, 1999; Jickells et al., 2005; Yu et al., 2015; Mahowald et al., 2017; Anderson, 2020). Apart from its impact on surface ocean biogeochemistry, mineral dust plays an important role in the Earth's climate by modifying radiation budget (Haywood et al., 2003; Kedia et al., 2018), cloud formation (Prenni et al., 2009; Koehler et al., 2009; Tang et al., 2019) and general atmospheric circulations (Evan et al., 2011). Also, dust storm episodes are considered as extreme events and can severely impact on human health (Giannadaki et al., 2014; Sarkar et al., 2019) as well as supply large amount of dust to remote locations (Aswini et al., 2020).

In the context of the Northern Indian Ocean (NIO), Arabian Peninsula (ARB) and Southwest Asia (SWA) are considered as major dust sources (Pease et al., 1998; Goudie and Middleton, 2006; Kumar et al., 2008; Badrinath et al., 2010; Ramaswamy et al., 2017; Aswini et al., 2020; Kumar et al., 2020) with occasional contribution from the Northeastern Africa (NEA) (Ackerman and Cox, 1989; Léon and Legrand, 2003; El-Askary et al., 2006). The Arabian Sea, located in the northwestern part of the NIO, receives a significant amount of mineral dust via wet and dry deposition processes ( $113\text{-}154\text{ Mtyr}^{-1}$ ) (Mahowald et al., 2005 references there within; Singh et al., 2008; Ramaswamy et al., 2017). The amount and nature of dust deposited over the Arabian Sea depends on regional meteorology characterized by strong reversal of seasonal winds, i.e., southwest (SW) monsoon (June to September) and northeast (NE) monsoon (October to January) (Nair, 2006; Glejin et al., 2012). The airborne mineral dust from various source region can further impact on the intensity of monsoon precipitation over India (Vinoj et al., 2014; Das et al., 2015). Among dry and wet deposition processes, later one is dominant during the SW monsoon (Ramaswamy et al., 2017). During the SW monsoon, atmospheric mineral dust is mainly transported at mid-tropospheric level (an altitude of 2-5 km) (Das et al., 2015; Ramaswamy et al., 2017), which potentially can have an adverse effect on the amount of precipitation and the rainwater chemistry (Ramaswamy et al., 2017). Tindale and Pease, (1999), during Joint Global Ocean Flux studies (JGOFS) program, have reported low ambient dust concentrations in the Arabian Sea, which essentially contribute to dry deposition, over the Arabian Sea during the SW monsoon. Recently, Ramaswamy et al. (2017) have reported on the significance of supply of mineral dust via wet deposition to the east coast of the Arabian Sea which averages around  $20\text{ g m}^{-2}\text{ yr}^{-1}$ . This flux is comparable or relatively higher than those estimated from sediment trap studies in the central and western Arabian Sea (Ramaswamy et al., 1991; Honjo et al., 1999). Post deposition, the role of these mineral dust is crucial as they supply several trace metals

and their isotopes along with the macro and micronutrients. The relative abundances of these trace metals also depend on sources from where these mineral dust particles are derived (Kumar et al., 2020). It is thus, important to characterize and identify the sources of long-range transported mineral dust which is supplied to surface water of the Arabian Sea to assess their impact on the biogeochemical processes.

Several studies have been attempted (Kumar et al., 2008; Kumar and Sarin, 2009; Kumar et al., 2012) to characterize the aerosols and their sources over the Arabian Sea. However, most of these studies have used elemental compositions as a tracer to identify its sources. In recent years, various studies have used naturally occurring radiogenic Sr and Nd isotopes as a robust tracer for identification of dust sources (Grousset and Biscaye, 2005; Meyer et al., 2011; 2013; Skonieczny et al. 2011; 2013; Abouchami et al. 2013; Kumar et al., 2015; 2018). Very recently, Kumar et al. (2020) have used radiogenic (Sr and Nd) isotopic ratios along with clay mineralogy and trace metal composition to characterize dust over the NEAS during dry period (October-May) and found their sources from the Arabian Peninsula, Southwest Asia, and the Thar Desert. They have also shown the transport pathways of mineral dust derived from different sources towards the Arabian Sea. In this study, we have measured Sr and Nd isotopic compositions, clay mineralogy, rare earth elements (REEs), and elemental composition of mineral dust collected from wet deposition at a coastal site located in the NEAS during the SW monsoon season of 2013. Our main objectives are (i) geochemical characterization of the wet deposited aeolian mineral dust over the NEAS as well as identify their sources and (ii) to assess temporal variability in sources of wet deposited mineral dust during the SW monsoon season. We have discussed about sampling site and analytical protocol in section 2. Results of geochemical and isotopic composition as well as varying air mass backtrajectories along with aerosol index maps and CALIPSO profile, during this study, is reported in section 3. Discussion on temporal variability in dust characteristics and identification of their possible sources using mixing models are detailed in section 4. The highlight of this study is summarized in last section with related implication of this study.

## **2. Sampling and analytical methods**

### **2.1 Site description and samples collection**

The wet deposition samples were collected on the terrace of a building located at the CSIR-National Institute of Oceanography (CSIR-NIO), Goa, (15° 45' N, 73° 80' E) during the SW monsoon (June to September) season of 2013 (Fig. 1). The major wind systems prevailing in this region during study period are the SW monsoon winds, which flow from the Indian Ocean over the

elevated East African coast and intensifies into Low Level Jet (LLJ) or Findlater Jet (Schott and McCarry, 2000). A strong northwesterly winds are typical feature over the Arabian Peninsula, also known as Summer Shamal (Yu. et. al., 2016), which is active from mid-May to mid-August as well as the Levar winds, which are mostly active from mid-May to mid-September, that flow from the central Asia towards the northern Arabian Sea through the active dust sources in the SW Asia (Sistan Basin, Makran coast and other deserts in the SW Asia (Ramaswamy et al., 2017). These major wind systems are active during SW monsoon period, (marked in magenta fonts in Fig. 1) which are responsible for dust outflow over the Arabian Sea. The sampling site is located at an altitude of 30 m from the sea level, and about 500 m away from the Arabian Sea coast (Fig 1; More detail on sampling site can be found in Kumar et al., (2020). To collect particulate matter from wet deposition, rainwater was collected using pre-cleaned (with Milli-Q water having resistivity = 18.2 M $\Omega$  cm) plastic trays during the study period. Rainwater was collected for 12-24 hours, depending on the intensity of precipitation on a particular sampling day. The wet deposition particulates (WDP) were extracted by filtering the collected rainwater samples using polycarbonate filters of 0.2  $\mu$ m pore size. The filtered WDP was allowed to dry (at room temperature) to remove water content, and subsequently used for processing and analyses of geochemical tracers. The detail of sample collection dates are mentioned in Table 1. The collected WDP samples (dominated by aeolian dust) were used to identify their sources using their clay mineralogy, REEs, major element composition, and Sr-Nd isotopic ratios.

## **2.2 Mineralogy of the wet deposition particulates**

Oriented glass slides for X-Ray diffraction (XRD) of 16 WDP samples were prepared by taking an aliquot of the samples collected on polycarbonate filters (during filtration), to which H<sub>2</sub>O<sub>2</sub> was added to remove the organic matter present in it. The deposited particles were made into a thick slurry and directly pipetted onto glass slides. The bulk mineralogy were done using Rigaku® Ultima IV XRD with Cu K $\alpha$  radiation at 40kV and 20mA between 3° - 30° 2 $\Theta$  at 0.02° 2 $\Theta$ /s. Semi-quantitative determination of mineral percentages was focused mainly on the clay minerals present in the samples. Illite, smectite, kaolinite, chlorite, and palygorskite were the major minerals identified. Peak areas were quantified by considering the area of a particular mineral above appropriate baseline using the Rigaku Integral analysis 6.0 software. The relative mineral percentages were evaluated using correction factors provided by Biscaye [1965].

### 2.3 Major elements, REEs and Sr-Nd isotopic analyses

Approximately 50 mg of filtered WDP were rinsed with Milli-Q (Merck Millipore) water to remove sea salt associated with it. Being collected from a location near to coastal region, it is expected to have a significant amount of sea-salt Sr, which can potentially imprint on mineral dust Sr composition (Kumar et al., 2020). Subsequently, the carbonate fraction was removed using an ammonium acetate buffered acetic-acid solution (pH = 5) by shaking for two hours (Kumar et al., 2020). The leaching step was repeated to assure that the samples were carbonate free. Subsequently, the supernatant residue was washed repetitively with deionized water and dried at 90 °C. The dried sample was further digested completely using a mixture of concentrated (Savillex double distilled) HF and HNO<sub>3</sub> acids in Savillex® PFA vials. This dried residue represents a pure silicate fraction of mineral dust. The digestion procedure was performed under a clean laminar flow bench at 110 °C for 24 hours and subsequently allowed to dryness. The HF-HNO<sub>3</sub> acid treatment was repeated once more to ensure complete digestion of particulate matter. Subsequent to dryness, all samples were re-dissolved using 2% supra-pure HNO<sub>3</sub> and stored in acid pre-cleaned polypropylene bottles for major and trace element analysis. Major elements were measured on ICP-OES (Agilent 710), while REE concentrations were measured using HR-ICP-MS (NU/ATTOM ES) at the National Institute of Oceanography, Goa. Few samples were analyzed repeatedly to determine the precision of analysis; these replicate measurements show analytical reproducibility of 5 % and 8 % for the major elements and REEs, respectively. To assess the accuracy of these measurements, international standards NIST (SRM 2710a Montana soil) was used as certified reference materials and the accuracy was found to be better than 8 % RSD for all trace elements. <sup>103</sup>Rh was used as an internal standard for performing the analysis.

In the silicate fractions of the WDP, pure form of Sr and Nd were extracted from the digested sample, and their isotopic compositions were measured following the protocol described in Kumar et al., (2020). In brief, approximately 50 mg of samples were taken and then leached with 1M ammonium acetate–acetic acid buffer solution at pH = 5 to remove the carbonate content. Subsequently, the samples were repeatedly washed with MQ water and then digested the silicate fractions completely using supra-pure conc. HF-HNO<sub>3</sub> acid mixture in PFA vials. Using the BioRad AG 50W-X8, (200-400 mesh) resin, Sr and REEs were separated. Eichrome ® LN resin (50-100 µm) was used to separate Nd isotopes from REEs fraction under the laminar flow bench (Kumar et al., 2020). Measurements of Sr and Nd isotopes were carried out using MC-ICP-MS (NU Plasma III), at National Institute of Oceanography, Goa. The obtained isotopic ratios were corrected for the

instrumental mass fractionation by normalizing the Sr and Nd isotopic data with  $^{86}\text{Sr}/^{88}\text{Sr}$  (= 0.1194) and  $^{146}\text{Nd}/^{144}\text{Nd}$  (= 0.7219) respectively. During the interval of these sample analysis, the isotopic composition of Sr and Nd of known international standards were also carried out. The average  $^{87}\text{Sr}/^{86}\text{Sr}$  ratio of standard SRM 987 during these measurements was  $0.710247 \pm 0.000021$  ( $2\sigma$ ,  $n = 22$ ) and  $^{143}\text{Nd}/^{144}\text{Nd}$  for Jndi1 standard solution was  $0.512095 \pm 0.000016$  ( $2\sigma$ ,  $n=20$ ) were obtained and which are consistent with their certified values (Peketi et al., 2020). Reagent blanks were also processed along with samples following the same procedure. The total procedural blanks for Sr and Nd were found to be negligible compared to the amount of these elements processed through the column chemistry. Therefore, no blank correction was done. Nd isotopic compositions were expressed as the deviation of the measured  $^{143}\text{Nd}/^{144}\text{Nd}$  of the Chondrite Uniform Reservoir (CHUR) ratio of 0.512638 (Jacobsen and Wasserburg, 1980) in parts per 10,000, defined as  $\epsilon_{\text{Nd}} = [((^{143}\text{Nd}/^{144}\text{Nd})_{\text{Sample}} / (^{143}\text{Nd}/^{144}\text{Nd})_{\text{CHUR}}) - 1] \times 10^4$ .

#### **2.4 Back trajectory and satellite data.**

Seven-day back trajectories ending at our sampling site were computed using HYSPLIT model (Draxler and Rolph, 2003) with the Global Data Assimilation System (GDAS) data, at different altitudes (i) 500-1500m (lower altitudes), (ii) 1500-3000m (mid altitude), and (iii) 3000-4500m (high altitude). These trajectories provide a synoptic picture of wind regimes during the study period. We retrieved UV-Aerosol Index data (<https://giovanni.gsfc.nasa.gov/giovanni/>) for the entire study region (including ARB, NEA, and SWA) to identify the active dust source regions during the sampling days. Also, we investigated CALIPSO (Cloud Aerosol Lidar Infrared Pathfinder Satellite Observations) profiles to specifically identify the presence of dust in the region (available online <https://www-calipso.larc.nasa.gov/>) for the satellite passing over or near the sampling site.

### **3. Results**

#### **3.1 Variation in back trajectories and dust profiles during SW Monsoon**

We computed seven day back trajectories and retrieved aerosol index data to broadly assess the source areas of the mineral dust which are active and can potentially contribute to dust collected at our sampling site during the study period. Back-trajectories (BT) along with aerosol index (AI) map for three wet deposition collection (WDP-1, 10, and 15) are shown in Fig. 2 (BT and AI for the rest of sampling days are detailed in Supplementary Material S1). We observed, from June to August 2013 of the study period, low-level trajectories originating from the Indian Ocean, which typically represents the SW monsoon winds (Fig. 2d). However, trajectories at higher altitudes are observed to

derive mainly from the north eastern Arabian Peninsula (Tigris-Euphrates floodplains and other deserts like Al-Nafud), which followed the Summer Shamal wind pathway and overrides the SW monsoon winds over the Gulf of Aden. For six sampling days (WDP-3, 4, 6, 9, 10, and 13), during June to August, the mid-altitude trajectories were also observed to originate from the northern Red Sea region, possibly indicating dust contribution from the coastal Red Sea sources. During September 2013, most trajectories (Fig. 2f) were found to originate from the northern and northeastern side of our sampling location, thus bringing dust mainly from the SW Asian sources including the Thar desert. Based on the wind pattern observed during the study period, we classified our samples in three categories namely (a) beginning of monsoon (BM): those collected in June-2013; (b) mid of monsoon (MM): those samples collected during July-August, 2013 and (c) end of the monsoon (EM): those collected during September 2013. Now onwards, we will discuss and interpret variability in dust sources based on this classification.

The Aerosol Index (AI) for all sampling days was examined over the different dust source regions, which complement our preliminary identification procedure. We observed high AI over the Gulf of Aden and the coastal regions of the ARB during sampling days of BM and MM (Fig. 2a and b). The back trajectories at higher altitudes passes over these regions may bring dust to our sampling site at the NEAS. At the EM (during September), back trajectories are mainly from the northern Arabian Sea region, indicating the change in the wind direction as there is a change in the wind system (retreating ITCZ). The AI for the EM samples shows high aerosol concentrations over the SWA, the northern Arabian Sea as well as ARB; however, wind regime suggests dust could be derived from SWA. The available CALIPSO images were also examined during the study period, along with AI. The vertical profiles show, dust transport mostly occurring at higher altitudes (2-5 Km) (Fig. 2g and h) during the SW monsoon, which is carried by the Shamal winds at the higher altitudes. The CALIPSO profiles, at the EM, shows mineral dust is mostly present in the NEAS since the dust in the EM is mainly from the SWA region by the retreating SW monsoon and Levar winds (Supplementary Material S1). The aerosol distribution from the closest overpass of CALIPSO profiles for the sampling days indicates the presence of a thick dust layer over the Arabian Sea upto 5 km height.

### **3.2 Mineralogy**

Major clay minerals observed in WDP samples are smectite (15-56%), illite (11-53%), and palygorskite (8-37 %) with moderate contribution from chlorite (10-29 %) and Kaolinite (10-22 %). A gradual increase in illite and chlorite concentration is observed with the highest contribution

during EM (average of illite = 49 % and chlorite = 25 %). However, no significant increase or decrease is found for kaolinite (Table-1). High illite and chlorite concentration are comparable with those observed for sources in the SWA, and moderate ones were similar to ARB sources (Sirocko and Lange, 1991; Kumar et al., 2020). A very high palygorskite (average = 33 %) content was observed for BM samples, which subsequently found to decrease in MM (19 %) and almost negligible in EM samples (Table-1). However, smectite is found to be highest during MM (average = 34 %) and low during BM and EM periods. The smectite content was found to be inversely correlated with palygorskite for all BM and MM samples (Fig. 4a). This considerable variation in relative percentage of clay minerals suggests significant temporal variability in dust composition and their sources impacting at the NEAS during the SW monsoon.

### **3.3 Major elements and REE patterns**

The major element and REEs concentrations of WDP of the year 2013 are summarized in Table-1 and Table-2. The relative abundances of major elements measured in decreasing order are Al>Fe>Mg>Ca>K>Ti>Mn. Al is the most abundant element (average of 6 %) varying from 3.9 to 7.5 %, followed by Fe (average of 4.5 %), which varied between 3.3 and 5.5 %. Mg and Ca were found to be varying from 1.4 to 3.2 % and 0.3 to 5.4 %, respectively. Al and other major element concentrations have been reported for potential dust sources of the Arabian Sea region (ARB; Kuwait, U.A.E, SWA; Iranian coast, Thar Desert) by Kumar et al., (2020), which were comparable (Al, Fe and Ca concentrations were 4.2%, 1.9%, and 10% respectively) with this study. Kumar et al. (2020), have also reported elemental composition for the soil samples collected from Kuwait and UAE., which are lower than those found in the BM samples (mainly derived from the ARB). This variation between the major elements in soil samples and the wet deposited dust may be due to the mixing of the dust from the other sources of the ARB during the mid-tropospheric transport in the SW monsoon months. In this study, major elements (Fe and Ti) were found to correlate significantly ( $r^2 = 0.75$ ;  $0.66$  respectively; see supplementary material S2) with Al (considered as a tracer for crustal sources; Kumar and Sarin, 2009) indicating their crustal origin. However, relatively poor correlation is found for Ca and Mg, similar to those observed for aerosols samples derived from the desert region as well as soil samples from source regions (Kumar et al., 2020).

The Post Archean Australian Shale (PAAS) normalized REE patterns of monthly averaged values for the wet deposition samples is given in Fig. 3, PAAS normalized patterns show the middle REE enrichment typically with a distinct positive Eu anomaly. The total REE values show an increasing trend from BM to MM and subsequently decreases towards the EM.



### 3.4. Sr-Nd isotopic compositions:

$^{87}\text{Sr}/^{86}\text{Sr}$  ratios and  $\epsilon_{\text{Nd}}$  values of the silicate fraction of the dust measured are presented in Table 1. The  $^{87}\text{Sr}/^{86}\text{Sr}$  ratios of WDP range from 0.7091 to 0.7193 during the study period. Relatively highly radiogenic  $^{87}\text{Sr}/^{86}\text{Sr}$  ratios (range: 0.7105-0.7131) were found for samples collected during BM (June), which tend to decrease towards MM (July and August) (range: 0.7091-0.7127) (Fig. 4c and Table-1). However, EM samples shows an increasing trend in Sr ratios with values reaching up to 0.7193 (Fig. 4c).  $\epsilon_{\text{Nd}}$  values of WDP silicate fraction found to vary from -2.3 to -9.1 during this study period. Relatively more radiogenic Nd has been observed in MM (average= -4.3) samples, however, relatively more negative  $\epsilon_{\text{Nd}}$  is found in BM (average= -6.0) and EM samples (average= -8.6). The  $\epsilon_{\text{Nd}}$  values show an opposite trend to that of the  $^{87}\text{Sr}/^{86}\text{Sr}$  ratios throughout the study period (Fig. 4c).

## 4. Discussion

### 4.1 Characterization and temporal variability of wet deposited dust over the NEAS

Elemental and mineralogical composition, particularly their ratios, are used to characterize dust from the source region (Usher et al., 2003; Kumar et al., 2020). These ratios are further used, in conjunction with the meteorological pattern, to trace sources of dust which undergo long-range transport to the remote oceanic and continental locations (Kumar and Sarin, 2009; Kumar et al., 2020). We used Fe/Al and Ti/Al ratios for characterization of collected WDP, which were found to vary from 0.65 to 1.08 and 0.06 to 0.10, respectively. A relatively homogeneous Fe/Al ratio is observed for BM ( $0.80\pm 0.12$ ), MM ( $0.74\pm 0.05$ ), and EM ( $0.81\pm 0.24$ ) samples, although enriched from the upper continental crustal (UCC) value (0.44; McLennan, 2001), indicating no significant temporal variability in deposited dust. Similarly, Ti/Al ratios did not exhibit any significant temporal variability (ratio for BM:  $0.09\pm 0.01$ ; MM:  $0.08\pm 0.01$  and EM:  $0.08\pm 0.02$ ). These observations suggest that elemental composition is not sufficient to decouple variation in sources and/or temporal variability as homogeneous ratios are observed for all collected dust particulates.

We investigated the composition of clay assemblage, including their ratios, extracted from the WDP, which are detailed in Table-1 and Supplementary Material S2 (Table-ST-1), respectively. The illite and chlorite abundance shows a steady increase from BM till EM, with insignificant variation in kaolinite content (Table 1). We used mineralogical ratios viz. illite/kaolinite (I/K), kaolinite/chlorite (K/C), and palygorskite/illite (P/I) (Supplementary Material S2; Table-ST-1) to characterize long-range transported dust (Kumar et al.; 2020). An increase in the I/K ratio, from BM

( $1.23 \pm 0.28$ ) to MM ( $1.44 \pm 0.48$ ) with highest in EM ( $3.22 \pm 1.16$ ), is observed during the SW monsoon period of 2013. This increase, possibly, hints to change in dust sources from the ARB to the SWA sources. A similar signature of I/K ratio have been reported by Kumar et al. (2020), wherein, higher I/K values (range: 1.8–7.3) were observed for aerosol samples sourced from the SWA compared to those sourced from ARB (Range: 1.0–1.3). In contrast, K/C values show the opposite trend, having the highest ratio ( $1.34 \pm 0.24$ ) during BM with gradual decrease in MM ( $1.04 \pm 0.28$ ) and EM ( $0.67 \pm 0.12$ ) (Fig. 4a and Table-ST-1). This contrast variation, between I/K and K/C ratios, have been observed by Kumar et al., (2020). A lower value of the K/C ratio indicates a contribution from SWA sources, which is also supported by ratios observed for Pakistan sediment sample (0.73; Svensson et al., (2000).

The BM and MM samples show significant palygorskite content with P/I ratio  $> 1$  (average BM:  $1.77 \pm 0.48$  and MM:  $1.04 \pm 0.28$ ), with the negligible contribution in EM sample (except one sample WDP-14 showing P/I = 0.3). Palygorskite minerals are commonly found in sabkha (supratidal, forming along arid coastlines that are characterised mainly by evaporite and carbonate deposits; Alharbi et al., 2016) and wadi (dry river beds rich in palygorskite in the Arabian Peninsula; Mackenzie et al., 1984) deposits in the ARB region as well as in the NEA (Debrabant et al., 1991, and references therein). A higher P/I ratio has been reported for surface sediments off the ARB and Horn of Africa-Gulf of Aden, significantly different from other regions in the Arabian Sea (Kolla et al., 1981). Also, Kumar et al., (2020), have used P/I ratio to distinguish ARB (range: 1.3-2.5) versus SWA sources for dust collected over the NEAS. Smectite percentages were observed high (range: 20-56%) during the MM period with the moderate presence in BM samples (range: 15-30 %) and negligible in EM samples (except in WDP-14). Various studies have shown the abundance of smectite in the NE African region due to the weathering of the Afar volcanic basalts (Sirocko and Lange 1991; Singer et al., 1998; Van Den Eeckhaut et al., 2009). The average of smectite in the sediments collected off the Horn of Africa is 40%, with palygorskite of 5-20%, which resemble the composition of our MM samples. In a recent study based on the marine sediments in the Gulf of Aden, Rojas, et al., (2019) have shown that the smectite and palygorskite are the major clay minerals present in the sediments, and are the mixture of sediments mainly derived from the Afar triangle and the ARB. The high smectite, moderate palygorskite, and illite in the MM samples possibly indicate mixed dust contributed from the NEA and ARB.

We further investigated the temporal variation of PAAS normalized REE pattern (Fig. 3), and we observed significant differences in  $\text{La}_n/\text{Yb}_n$  ratio and  $\text{Eu}/\text{Eu}^*$  anomaly displayed in Fig. 4b.

Typically,  $La_n/Yb_n$  ratio represents the abundance of light REE (LREE) versus heavy REE (HREE), wherein lower the  $La_n/Yb_n$  indicates enrichment of HREE in the samples. Enrichment in LREE and HREE is commonly derived from acidic and alkaline rocks, respectively (McLennan, 1989).  $La_n/Yb_n$  ratio for the samples collected at the BM is more than one and this tends to decrease towards MM samples (July and August). Subsequently, we observe an increased value in EM samples (September), reaching up to 1.3. This shows an abundance of aeolian dust enriched in HREE within MM samples. Similar HREEs enrichment is found for basic rocks from the NE African region (McLennan 1989), suggesting their possible contribution to MM samples. However, LREE enrichment is observed for BM and EM samples reflecting the contribution from different sources other than NEA. One of the REE fractionations, due to geological processes, is also expressed in terms of  $Eu/Eu^*$  anomaly, which mainly depends on the type of parent rocks (Bau, 1991). Relatively high  $Eu$  anomaly (Average: 1.126; Range: 1.090-1.170) is observed in MM samples compared to BM (Average: 1.109; Range: 1.081-1.139) and EM (Average: 1.101; Range: 1.043-1.181) samples. This further highlights different sources impacting WDP abundance in the three sets of samples. The scatter plot between  $Eu/Eu^*$  and  $La_n/Yb_n$  (See supplementary material S3) provides the difference in the source rock of the dust, which is helpful for source characterization (Nakai et al., 1993; Sun 2002; Muhs et al., 2007). We observed two different clusters having July and August samples in one and June and September samples in other. We did observe June end samples overlapping with MM cluster, possibly indicating inherent similarity in  $Eu$  anomaly of dust samples.

Temporal variation in the Sr-Nd isotopic composition shows the least radiogenic  $^{87}Sr/^{86}Sr$  (average:  $0.7112 \pm 0.0011$ ) and highly radiogenic  $\epsilon_{Nd}$  (average:  $-4.3 \pm 0.9$ ) during MM (Table-1). In contrast, relatively high radiogenic  $^{87}Sr/^{86}Sr$  is found for BM (average:  $0.7118 \pm 0.0012$ ) and EM (average:  $0.7156 \pm 0.0034$ ) samples. Similarly,  $\epsilon_{Nd}$  shows a very distinct signature for BM (average:  $-6.0 \pm 1.25$ ) and EM samples (average:  $-8.6 \pm 0.7$ ), clearly highlighting the role of distinct source impacting the WDP collected in the year 2013. BM samples, except WDP-4, are showing characteristic isotopic signature similar to those of dust sourced from ARB ( $^{87}Sr/^{86}Sr = 0.709-0.714$  and  $\epsilon_{Nd} = -7.8$  to  $-6.0$ ) reported by Kumar et al., (2020) and Sirocko (1995). These samples also have high Palygorskite content supporting their origin from ARB. The characteristic isotopic composition of MM samples shows relatively large variability in  $\epsilon_{Nd}$  values, with highly radiogenic  $\epsilon_{Nd}$  ( $-2.7$ ) and tends to decrease towards EM. The isotopic signature of some of the MM samples (WDP-7, 8, 9, 10, and 11) are different than those reported for the ARB and SWA by Kumar et al. (2020), suggesting the contribution from a different source impacting to the Arabian Sea during SW Monsoon. The arid/semi-arid region in the NEA may be a potential source for dust that possibly gets carried along

with Findlater Jet, augmented by Red sea winds during SW monsoon (Ramaswamy et al., 2017). The NEA desert region is mainly composed of Cenozoic alkali basalts, which are the major source of the sediments in the Afar region (located in the parts of Ethiopia, Eritria and Djibouti) with the high radiogenic  $\epsilon_{Nd}$  values (0 to +10) and relatively low  $^{87}Sr/^{86}Sr$  ratios (0.703 to 0.705) (Betton and Civetta, 1984; Teklay et al., 2009; Ayalew et al., 2018). It is important to state here, ARB source is active during this period and can contribute significantly, which is also supported by air-mass back trajectories deriving from ARB. A mixed isotopic signature is thus, observed for WDP-5, 6, 7, 12, and 13 (Fig. 4c), which is also supported by relatively low palygorskite content compared to BM samples (Table-1). Towards the EM, we observed highly radiogenic  $^{87}Sr/^{86}Sr$  (value goes up to 0.7194) and relatively lower  $\epsilon_{Nd}$  values (-9.1). The isotopic signature for EM samples compare with those dust derived from the SWA region ( $^{87}Sr/^{86}Sr = 0.714-0.720$  and  $\epsilon_{Nd} = -20.1$  to  $-7.4$ ) reported by Kumar et al., (2020). Almost negligible palygorskite and smectite, along with an increase in illite and chlorite content in EM samples, supports dust sourced from the SWA region.

Overall, based on isotopic, mineralogical, and REEs characteristics, we observed significant temporal variability in WDP over the NEAS during SW monsoon. These dust particles are found to be derived from three major sources i) ARB ii) NEA and iii) SWA. It is important to mention here, the temporal variability reported here, is based on one year data. The robustness of this temporal variability can be further ascertained by analyzing long-term (4-5 years) geochemical proxies of mineral dust at coastal locations over the NEAS.

#### **4.2 Provenances of dust over the NEAS during the SW monsoon**

The mineral dust is the weathered product of the bedrocks in the arid and semi-arid (source) region, and their isotopic signatures are mostly contributed by the bedrocks (Grouseet et al., 2005). So different geological settings in bedrocks of source region contribute to the distinct isotopic signatures, which can be used to characterize and identify the provenance of dust from various sources. The Sr and Nd isotopic composition of WDP collected in 2013 are plotted in Fig. 5, along with the fields (characterized by their average composition) of four different potential sources, which can contribute to dust over the Arabian Sea. The average Sr-Nd composition and their concentration are based on the data available in the literature (Sirocko, 1995; Tripathi et al., 2004; Ferrat et al., 2011; Ayalew et al., 2018; Kumar et al., 2020) are summarized in Table-3. Samples collected at the BM (WDP-1, 2, and 3) show highly radiogenic  $^{87}Sr/^{86}Sr$  and less radiogenic  $\epsilon_{Nd}$ , which are found to cluster in the ARB field. These compositions found in the range of isotopic composition of aerosol sourced from the dust storms over the ARB ( $^{87}Sr/^{86}Sr = 0.7175$ ;  $\epsilon_{Nd} = -7.5$ ) reported by Kumar et al.,

(2020). However, WDP-4 is found to lie away from this field and towards the NEA field indicating contribution from the NEA sources. We also observed high palygorskite (with moderate smectite) abundance in BM samples, which supports to their source from ARB (Sirocko et al., 1991a, b), without ambiguity. However, relatively lower palygorskite content is found for WDP-4, with simultaneous increase in smectite abundance indicate contribution from the NEA source region. The strong north-northwesterly Summer Shamal winds which blow over the Arabian Peninsula towards the Gulf of Aden, from the end of May to mid-August plays a major role in transporting the dust towards the Arabian Sea (Ramaswamy et al., 2017; Yu et al., 2016) (Fig. 1). Considering ARB as one of the end members (Table-3) and NEA as other (Table-3), a mixing model representing fractional contribution from each end member can be drawn (Fig. 5), following mixing equations by Faure and Mensing, (2005). We observed, most of the BM samples are falling near and/or on this mixing line, and a dominant contribution (more than 80 %) can be apportioned to ARB sources (Fig. 5).

Similar to BM samples, we observed the majority of MM samples (except WDP-8 and 10), tend to fall in or on the edge of ARB space (Fig. 5), however, tending towards the NEA end-member. These samples have relatively high smectite with moderate palygorskite content, which is distinct from BM samples. Yet, being near the mixing line between ARB and NEA, a dominant contribution from ARB can be ascertained to most of the MM samples. This interpretation is also supported by inferences drawn from back trajectory analyses and CALIPSO retrievals (see section 3.1 and Supplementary Material 1), which both highlight intense dust activity over ARB during the MM period of 2013, during which winds will be carrying dust from ARB and overriding on SW monsoon winds. In contrast, WDP-8 and 10, fall away from the ARB source, although on or near the NEA-ARB mixing line (Fig. 5), and are therefore not exclusively sourced from the ARB. These two samples show a gradual increase in  $\epsilon_{Nd}$  associated with a small decrease in  $^{87}Sr/^{86}Sr$  and tend to plot towards the NEA source. In addition, we observed high smectite followed by palygorskite content, which indicates the increased contribution from the NEA sources (Sirocko et al., 1991a, b; Rojas et al., 2019). Similarly high smectite is found for few MM samples, which is identified to be dominantly contributed by the NEA based on Sr-Nd isotopic composition. Thus a mixed contribution from ARB and NEA can be attributed to MM samples collected during the southwest monsoon. Back trajectories for the samples collected in the MM, shows the air masses passing over the NEA sources as well as the ARB sources. The end member mixing curve between NEA and ARB (shown in Fig. 5) suggests 30-50 % of dust contribution from NEA sources for the MM samples, which have highly radiogenic  $\epsilon_{Nd}$  (WDP-8 and 10).

WDP samples (WDP-14, 15 and 16) collected in September, 2013 exhibit relatively highly radiogenic  $^{87}\text{Sr}/^{86}\text{Sr}$  (average  $^{87}\text{Sr}/^{86}\text{Sr} = 0.7156$ ) and relatively less radiogenic  $\epsilon_{\text{Nd}}$  (average  $\epsilon_{\text{Nd}} = -8.6$ ), tend to plot away from ARB source and towards the SWA (WDP-14) and Thar Desert (WDP-15 and 16) source (Fig. 5). We also observed insignificant palygorskite and smectite (except WDP-14) in the EM samples, suggesting a decreased and/or negligible contribution from ARB source. In addition, we found a high abundance of illite and chlorite, a characteristic feature of SWA (Alizai et al., 2012) and Thar Desert (Kumar et al., 2020). During EM (September), the wind blows from north to south as the ITCZ starts migrating towards the south, and the Shamal winds cease to exist (Yu et al., 2016). In contrast, the Levar winds blow through the Sistan basin, Makran coast in the Northern Arabian Sea till September (Alizadeh Choobari et al., 2014). The northern Levar winds are strong enough to raise the dust from the SW Asian dust sources and transport it to the Arabian Sea. Using the end-member mixing equation for ARB and SWA, more than 60 % contribution from SWA can be attributed to WDP-14. However, the absence of palygorskite and smectite in WDP- 15 and 16 infer to insignificant contribution from ARB and mainly dominated by Thar Desert source. Our interpretation of source identification is based on the geochemical characteristic data available for aerosols samples and soil samples; however, to make more robust conclusions for dust provenance, the isotopic composition of soil samples from the source region, particularly from SWA source is crucial.

## 5. Summary and implications

We report geochemical (major element, REEs, clay mineralogy, and Sr-Nd isotopic ratio) composition of wet deposited particles, collected at a costal station located in the NEAS during southwest monsoon period of 2013. During SW Monsoon, majority of dust reaches the Eastern Arabian Sea via mid-tropospheric transport and undergoes wet deposition, which can significantly impact on surface ocean biogeochemical processes. Based on changing wind regime, collected samples are classified into the beginning of Monsoon (BM; June); mid of Monsoon (MM; July and August) and end of Monsoon (EM; September). The elemental composition and their ratios (particularly Fe/Al and Ti/Al) did not show any significant temporal variability during this study period. In contrast, significant temporal variability is observed for clay mineralogical composition with an increasing value of illite and chlorite starting from BM till EM samples. The temporal variability is also observed in palygorskite and smectite abundance suggesting variation in dust sources impacting the NEAS during SW Monsoon. High palygorskite and moderate smectite are found in BM and the majority of MM samples. However, few MM samples show high smectite and

moderate palygorskite abundance, and the absence of both palygorskite and smectite, in EM samples highlights the change in the provenance of dust during SW Monsoon. In addition to clay minerals, we also observed significant difference in  $La_n/Yb_n$  ratio with lower values found for MM samples compared to those for BM and EM samples (more than 1). Relatively high  $Eu/Eu^*$  is observed for MM samples compared to BM and EM samples, inferring to change in dust sources during the study period.

In addition to clay mineralogy and REEs pattern, we assessed variation in radiogenic isotopic (Sr and Nd) composition for wet deposited dust and a significant temporal variation is observed for isotopic ratios with less radiogenic  $^{87}Sr/^{86}Sr$  and relatively more radiogenic  $\epsilon_{Nd}$  signature are shown by MM samples compared to BM and EM samples. These variations clearly highlights the role of source region activation and subsequent emission impact the dust characteristics and composition at the receptor region. We further attempted to assess the relative contribution from different sources using endmember mixing calculations by defining several end-members (ARB, NEA, SWA, and the Thar Desert). The End-member mixing calculations indicate more than 80 % contribution of ARB to BM and majority of MM samples, the mixed contribution from NEA and ARB towards a few of MM samples and SWA and Thar Desert contribution to EM samples. These source attributions are also supported by clay mineralogical composition as well as back trajectories and satellite data.

This reported data set on the geochemical composition of WDP is the first one from this region, fulfilling a major gap in understanding the impact of dust deposition to surface water biogeochemical processes in the Arabian Sea. Most of the precipitation over the Indian sub-continent occurs during the SW monsoon and is very significant from the socio-economical perspective. Several studies have highlighted the vital role of long-range transported dust on the SW monsoon intensity and their outbreak (Vinoj et al., 2014; Das et al., 2015). Any changes in the dust emission from the source regions may modulate the rainfall intensity and pattern over the Indian sub-continent. In order to understand the changing pattern of dust emission from the source region, it is important to characterize dust and identify their sources, which makes this study very crucial. We have clearly shown significant temporal variability in the dust characteristics, which is dependent on the wind pattern as well as dust activity/emission in the source region. The dust particles which are getting removed via wet/dry deposition can significantly impact continental (Ramaswamy et al., 2017 and reference therein) and oceanic ecosystem (Swap et al., 1992; Prospero 1999, Mahowald, et al., 2011, Guieu et al., 2019). The deposition flux and their impact depends on the type of dust which eventually depend on the emitting sources, thus, making this study relevant. The information on dust

characteristics and their sources via wet deposition is relevant for the data interpretation of marine sedimentary records to better understand mineral dust cycle in the past and its role in the paleo-productivity

### **Acknowledgment:**

Funding for this research is supported by CSIR Networked Project GEOSINK. The Department of Science and Technology funded Ashwini Kumar, K Suresh, and Udisha Singh, Govt. of India, under the INSPIRE Faculty scheme (IFA13-EAS-13), INSPIRE Research Fellowship (IF140405) and (IF180350) respectively. We thank Mr. Arvind Shukla and Mr. Robin John for support during analyses of isotopic composition and REEs, respectively. We gratefully acknowledge the NOAA Air Resources Laboratory (ARL) for the provision of the HYSPLIT transport and dispersion model (<http://www.ready.noaa.gov>) used in this publication.

### **References**

- Abouchami, W., N  the, K., Kumar, A., Galer, S. J., Jochum, K. P., Williams, E., & Mezger, K. (2013). Geochemical and isotopic characterization of the Bod  l   Depression dust source and implications for transatlantic dust transport to the Amazon Basin. *Earth and Planetary Science Letters*, 380, 112-123.
- Ackerman, S. A., & Cox, S. K. (1989). Surface weather observations of atmospheric dust over the southwest summer monsoon region. *Meteorology and Atmospheric Physics*, 41(1), 19-34.
- Alizadeh-Choobari, O., Zawar-Reza, P., & Sturman, A. (2014). The “wind of 120 days” and dust storm activity over the Sistan Basin. *Atmospheric research*, 143, 328-341.
- Alizai, A., Hillier, S., Clift, P. D., Giosan, L., Hurst, A., VanLaningham, S., & Macklin, M. (2012). Clay mineral variations in Holocene terrestrial sediments from the Indus Basin. *Quaternary Research*, 77(3), 368-381.
- Alharbi, O.A., Williams, A.T., Phillips, M.R. et al. Textural characteristics of sediments along the southern Red Sea coastal areas, Saudi Arabia. *Arab J Geosci* 9, 735 (2016). <https://doi.org/10.1007/s12517-016-2741-y>
- Anderson, R. F., (2020). GEOTRACES: Accelerating Research on the Marine Biogeochemical Cycles of Trace Elements and Their Isotopes. *Annual Review of Marine Science*, 12, 49-85.
- Aswini, M. A., Kumar, A., & Das, S. K. (2020). Quantification of long-range transported aeolian dust towards the Indian peninsular region using satellite and ground-based data-A case study during a dust storm over the Arabian Sea. *Atmospheric Research*, 239, 104910.
- Ayalew, D., Jung, S., Romer, R. L., & Garbe-Sch  nberg, D. (2018). Trace element systematics and Nd, Sr and Pb isotopes of Pliocene flood basalt magmas (Ethiopian rift): A case for Afar plume-lithosphere interaction. *Chemical Geology*, 493, 172-188.



- Badarinath, K.V.S.; Kharol, S.K.; Kaskaoutis, D.G.; Sharma, A.R.; Ramaswamy, V.; Kambezidis, H.D. (2010). Long-range transport of dust aerosols over the Arabian Sea and Indian region – A case study using satellite data and ground-based measurements. *Global Planet. Change*: 72(3); 2010; 164-181.
- Bau, M. (1991). Rare-earth element mobility during hydrothermal and metamorphic fluid-rock interaction and the significance of the oxidation state of europium. *Chemical Geology*, 93(3-4), 219-230.
- Betton, P. J., & Civetta, L. (1984). Strontium and neodymium isotopic evidence for the heterogeneous nature and development of the mantle beneath Afar (Ethiopia). *Earth and planetary science letters*, 71(1), 59-70.
- Biscaye, P. E. (1965). Mineralogy and sedimentation of recent deep-sea clay in the Atlantic Ocean and adjacent seas and oceans. *Geological Society of America Bulletin*, 76(7), 803-832.
- Das, S., Dey, S., Dash, S. K., Giuliani, G., & Solmon, F. (2015). Dust aerosol feedback on the Indian summer monsoon: Sensitivity to absorption property. *Journal of Geophysical Research: Atmospheres*, 120(18), 9642-9652.
- Debrabant, P., Krissek, L., Bouquillon, A., & Chamley, H. (1991). Clay mineralogy of Neogene sediments of the western Arabian Sea: mineral abundances and paleoenvironmental implications. In *Proceedings of the ocean drilling program, Scientific Results (Vol. 117, pp. 183-186)*. College Station, TX: (Ocean Drilling Program).
- Draxler, R. R., & Rolph, G. D. (2003). HYSPLIT (HYbrid Single-Particle Lagrangian Integrated Trajectory) model access via NOAA ARL READY website (<http://www.arl.noaa.gov/ready/hysplit4.html>). NOAA Air Resources Laboratory, Silver Spring.
- El-Askary, H. (2006). Air pollution impact on aerosol variability over mega cities using remote sensing technology: case study, Cairo, Egypt. *Egyptian Journal of Remote Sensing & Space Science*, 9, 31-40.
- Evan, A. T., Foltz, G. R., Zhang, D., & Vimont, D. J. (2011). Influence of African dust on ocean-atmosphere variability in the tropical Atlantic. *Nature Geoscience*, 4(11), 762-765.
- Faure, G., & Mensing, T. M. (2005). *Principles and applications* (p. 897). John Wiley & Sons, Inc.
- Ferrat, M., Weiss, D. J., Strekopytov, S., Dong, S., Chen, H., Najorka, J., ... & Sinha, R. (2011). Improved provenance tracing of Asian dust sources using rare earth elements and selected trace elements for palaeomonsoon studies on the eastern Tibetan Plateau. *Geochimica et Cosmochimica Acta*, 75(21), 6374-6399.
- Giannadaki, D., Pozzer, A., & Lelieveld, J. (2014). Modeled global effects of airborne desert dust on air quality and premature mortality. *Atmospheric Chemistry & Physics*, 14(2).
- Glejin, J., V Sanil, K., Sajiv Philip, C., Jai, S., Premanand, P., K Ashok, K., ... & Rajamanickam, G. (2012). Variations in swells along eastern Arabian Sea during the summer monsoon. *Open Journal of Marine Science*, 2012.

- Goudie, A. S., & Middleton, N. J. (2006). Desert dust in the global system. Springer Science & Business Media.
- Grousset, F. E., & Biscaye, P. E. (2005). Tracing dust sources and transport patterns using Sr, Nd and Pb isotopes. *Chemical Geology*, 222(3-4), 149-167.
- Guieu, C., Al Azhar, M., Aumont, O., Mahowald, N., Lévy, M., Éthé, C., & Lachkar, Z. (2019). Major impact of dust deposition on the productivity of the Arabian Sea. *Geophysical Research Letters*, 46(12), 6736-6744.
- Haywood, J., Francis, P., Osborne, S., Glew, M., Loeb, N., Highwood, E., ... & Hirst, E. (2003). Radiative properties and direct radiative effect of Saharan dust measured by the C-130 aircraft during SHADE: 1. Solar spectrum. *Journal of Geophysical Research: Atmospheres*, 108(D18).
- Honjo, S., Dymond, J., Prell, W., & Ittekkot, V. (1999). Monsoon-controlled export fluxes to the interior of the Arabian Sea. *Deep Sea Research Part II: Topical Studies in Oceanography*, 46(8-9), 1859-1902.
- Jacobsen, S. B., & Wasserburg, G. J. (1980). Sm-Nd isotopic systematics of chondrites and achondrites. *Meteoritics*, 15, 307.
- Jickells, T. D., An, Z. S., Andersen, K. K., Baker, A. R., Bergametti, G., Brooks, N., ... & Kawahata, H. (2005). Global iron connections between desert dust, ocean biogeochemistry, and climate. *science*, 308(5718), 67-71.
- Kedia, S., Kumar, R., Islam, S., Sathe, Y., & Kaginalkar, A. (2018). Radiative impact of a heavy dust storm over India and surrounding oceanic regions. *Atmospheric Environment*, 185, 109-120.
- Koehler, K. A., DeMott, P. J., Kreidenweis, S. M., Popovicheva, O. B., Petters, M. D., Carrico, C. M., ... & Shonija, N. K. (2009). Cloud condensation nuclei and ice nucleation activity of hydrophobic and hydrophilic soot particles. *Physical Chemistry Chemical Physics*, 11(36), 7906-7920.
- Kolla, V., KostECKI, J. A., Robinson, F., Biscaye, P. E., & Ray, P. K. (1981). Distributions and origins of clay minerals and quartz in surface sediments of the Arabian Sea. *Journal of Sedimentary Research*, 51(2), 563-569.
- Kumar, A., & Sarin, M. M. (2009). Mineral aerosols from western India: Temporal variability of coarse and fine atmospheric dust and elemental characteristics. *Atmospheric Environment*, 43(26), 4005-4013.
- Kumar, A., Abouchami, W., Galer, S. J. G., Garrison, V. H., Williams, E., & Andreae, M. O. (2014). A radiogenic isotope tracer study of transatlantic dust transport from Africa to the Caribbean. *Atmospheric Environment*, 82, 130-143.
- Kumar, A., Abouchami, W., Galer, S. J. G., Singh, S. P., Fomba, K. W., Prospero, J. M., & Andreae, M. O. (2018). Seasonal radiogenic isotopic variability of the African dust outflow to the tropical Atlantic Ocean and across to the Caribbean. *Earth and Planetary Science Letters*, 487, 94-105.

- Kumar, A., Sarin, M. M., & Sudheer, A. K. (2008). Mineral and anthropogenic aerosols in Arabian Sea–atmospheric boundary layer: Sources and spatial variability. *Atmospheric Environment*, 42(21), 5169-5181.
- Kumar, A., Sudheer, A. K., Goswami, V., & Bhushan, R. (2012). Influence of continental outflow on aerosol chemical characteristics over the Arabian Sea during winter. *Atmospheric Environment*, 50, 182-191.
- Kumar, A., Suresh, K., & Rahman, W. (2020). Geochemical characterization of modern aeolian dust over the Northeastern Arabian Sea: Implication for dust transport in the Arabian Sea. *Science of The Total Environment*, 138576.
- Léon, J. F., & Legrand, M. (2003). Mineral dust sources in the surroundings of the north Indian Ocean. *Geophysical Research Letters*, 30(6).
- Mackenzie, R.C., M.J. Wilson, A.S. Mashhady (1984). Origin of Palygorskite in Some Soils of the Arabian Peninsula, Book chapter in *Developments in Sedimentology*, Editor(s): A. Singer, E. Galan, 37, 177-186, Elsevier
- Mahowald, N. M., Baker, A. R., Bergametti, G., Brooks, N., Duce, R. A., Jickells, T. D., ... & Tegen, I. (2005). Atmospheric global dust cycle and iron inputs to the ocean. *Global biogeochemical cycles*, 19(4).
- Mahowald, N. M., Scanza, R., Brahney, J., Goodale, C. L., Hess, P. G., Moore, J. K., & Neff, J. (2017). Aerosol deposition impacts on land and ocean carbon cycles. *Current Climate Change Reports*, 3(1), 16-31.
- Mahowald, N., Ward, D. S., Kloster, S., Flanner, M. G., Heald, C. L., Heavens, N. G., ... & Chuang, P. Y. (2011). Aerosol impacts on climate and biogeochemistry. *Annual review of environment and resources*, 36.
- McLennan, S. M. (1989). Rare earth elements in sedimentary rocks: influence of provenance and sedimentary processes. *Geochemistry and Mineralogy of Rare Earth Elements, Reviews in Mineralogy* 21, 169-200.
- McLennan, S. M. (2001). Relationships between the trace element composition of sedimentary rocks and upper continental crust. *Geochemistry, Geophysics, Geosystems*, 2(4).
- Meyer, I., Davies, G. R., & Stuut, J. B. W. (2011). Grain size control on Sr-Nd isotope provenance studies and impact on paleoclimate reconstructions: An example from deep-sea sediments offshore NW Africa. *Geochemistry, Geophysics, Geosystems*, 12(3).
- Meyer, I., Davies, G. R., Vogt, C., Kuhlmann, H., & Stuut, J. B. W. (2013). Changing rainfall patterns in NW Africa since the Younger Dryas. *Aeolian Research*, 10, 111-123.
- Muhs, D. R., Budahn, J. R., Prospero, J. M., & Carey, S. N. (2007). Geochemical evidence for African dust inputs to soils of western Atlantic islands: Barbados, the Bahamas, and Florida. *Journal of Geophysical Research: Earth Surface*, 112(F2).
- Nair, T. B. (2006). Monsoon control on trace metal fluxes in the deep Arabian Sea. *Journal of earth system science*, 115(4), 461-472.

- Nakai, S. I., Halliday, A. N., & Rea, D. K. (1993). Provenance of dust in the Pacific Ocean.
- Pease, P. P., Tchakerian, V. P., & Tindale, N. W. (1998). Aerosols over the Arabian Sea: geochemistry and source areas for aeolian desert dust. *Journal of Arid Environments*, 39(3), 477-496.
- Peketi, A., Mazumdar, A., Pillutla, S. P. K., Rai, V. K., Sawant, B., & Chaitanya, A. V. S. (2020). Monsoon rainfall and contrasting source rocks influenced sediment composition of peninsular basins along the east coast of India (western Bay of Bengal). *Marine and Petroleum Geology*, 104433.
- Prenni, A. J., Petters, M. D., Kreidenweis, S. M., Heald, C. L., Martin, S. T., Artaxo, P., ... & Pöschl, U. (2009). Relative roles of biogenic emissions and Saharan dust as ice nuclei in the Amazon basin. *Nature Geoscience*, 2(6), 402-405.
- Prospero, J. M. (1999). Long-range transport of mineral dust in the global atmosphere: Impact of African dust on the environment of the southeastern United States. *Proceedings of the National Academy of Sciences*, 96(7), 3396-3403.
- Ramaswamy, V., Muraleedharan, P. M., & Babu, C. P. (2017). Mid-troposphere transport of Middle-East dust over the Arabian Sea and its effect on rainwater composition and sensitive ecosystems over India. *Scientific reports*, 7(1), 1-8.
- Ramaswamy, V., Nair, R. R., Manganini, S., Haake, B., & Ittekkot, V. (1991). Lithogenic fluxes to the deep Arabian Sea measured by sediment traps. *Deep Sea Research Part A. Oceanographic Research Papers*, 38(2), 169-184.
- Rashki, A., Kaskaoutis, D.G., Mofidi, A., Minvielle, F., Chiapello, I., Legrand, M., Dumka, U.C., Francois, P., 2019. Effects of Monsoon, Shamal and Levar winds on dust accumulation over the Arabian Sea during summer – the July 2016 case. *Aeolian Res.*36, 27–44. <https://doi.org/10.1016/j.aeolia.2018.11.002>.
- Rojas, V. P., Meynadier, L., Colin, C., Bassinot, F., Valet, J. P., & Miska, S. (2019). Multi-tracer study of continental erosion and sediment transport to the Red Sea and the Gulf of Aden during the last 20 ka. *Quaternary Science Reviews*, 212, 135-148.
- Sarkar, S., Chauhan, A., Kumar, R., & Singh, R. P. (2019). Impact of deadly dust storms (May 2018) on air quality, meteorological, and atmospheric parameters over the northern parts of India. *GeoHealth*, 3(3), 67-80.
- Schott and McCarty (2005). *The Monsoon Circulation of the Indian Ocean. Progress in Oceanography*
- Singer, A., Stahr, K., & Zarei, M. (1998). Characteristics and origin of sepiolite (Meerschaum) from Central Somalia. *Clay Minerals*, 33(2), 349-362.
- Singh, R. P., Prasad, A. K., Kayetha, V. K., & Kafatos, M. (2008). Enhancement of oceanic parameters associated with dust storms using satellite data. *Journal of Geophysical Research: Oceans*, 113(C11).
- Sirocko, F. (1995). Abrupt changes in monsoon climate: evidences from the geochemical composition of Arabian Sea sediment, *Habilitations Thesis, Univ. Kiel, Germany*, 216.

- Sirocko, F., & Lange, H. (1991a). Clay-mineral accumulation rates in the Arabian Sea during the late Quaternary. *Marine Geology*, 97(1-2), 105-119.
- Sirocko, F., Sarnthein, M., Lange, H., & Erlenkeuser, H. (1991). Atmospheric summer circulation and coastal upwelling in the Arabian Sea during the Holocene and the last glaciation. *Quaternary Research*, 36(1), 72-93.
- Skonieczny, C., Bory, A., Bout-Roumazeilles, V., Abouchami, W., Galer, S. J. G., Crosta, X., ... & Ndiaye, T. (2013). A three-year time series of mineral dust deposits on the West African margin: sedimentological and geochemical signatures and implications for interpretation of marine paleo-dust records. *Earth and Planetary Science Letters*, 364, 145-156.
- Skonieczny, C., Bory, A., Bout-Roumazeilles, V., Abouchami, W., Galer, S. J., Crosta, X., ... & Chatenet, B. (2011). The 7–13 March 2006 major Saharan outbreak: Multiproxy characterization of mineral dust deposited on the West African margin. *Journal of Geophysical Research: Atmospheres*, 116(D18).
- Sun, J. (2002). Provenance of loess material and formation of loess deposits on the Chinese Loess Plateau. *Earth and planetary science letters*, 203(3-4), 845-859.
- Svensson, A., Biscaye, P. E., & Grousset, F. E. (2000). Characterization of late glacial continental dust in the Greenland Ice Core Project ice core. *Journal of Geophysical Research: Atmospheres*, 105(D4), 4637-4656.
- Swap, R., Garstang, M., Greco, S., Talbot, R., & Källberg, P. (1992). Saharan dust in the Amazon Basin. *Tellus B*, 44(2), 133-149.
- Tang, W., Yang, K., Qin, J., Li, X., & Niu, X. (2019). A 16-year dataset (2000–2015) of high-resolution (3 h, 10 km) global surface solar radiation. *Earth System Science Data*, 11(4).
- Teklay, M., Scherer, E., Mezger, K., Danyushevsky, L., (2009). Geochemical characteristics and Sr-Nd-Hf isotope compositions of mantle xenoliths and host basalts from Assab, Eritrea: implications for the composition and thermal structure of the lithosphere beneath the Afar Depression. *Contrib. Mineral. Petrol.* 159,731-751.
- Tindale, N. W., & Pease, P. P. (1999). Aerosols over the Arabian Sea: Atmospheric transport pathways and concentrations of dust and sea salt. *Deep Sea Research Part II: Topical Studies in Oceanography*, 46(8-9), 1577-1595.
- Tripathi, J. K., Bock, B., Rajamani, V., & Eisenhauer, A. (2004). Ca and Sr dynamics in the Indo-Gangetic plains: Different sources and mobilization processes in northwestern India. *Current Science*, 1453-1458.
- Usher, C. R., Michel, A. E., & Grassian, V. H. (2003). Reactions on mineral dust. *Chemical Reviews*, 103(12), 4883-4940.
- Van Den Eeckhaut, M., Moeyersons, J., Nyssen, J., Abraha, A., Poesen, J., Haile, M., & Deckers, J. (2009). Spatial patterns of old, deep-seated landslides: A case-study in the northern Ethiopian highlands. *Geomorphology*, 105(3-4), 239-252.

Vinoj, V., Rasch, P. J., Wang, H., Yoon, J. H., Ma, P. L., Landu, K., & Singh, B. (2014). Short-term modulation of Indian summer monsoon rainfall by West Asian dust. *Nature Geoscience*, 7(4), 308-313.

Yu, H., Chin, M., Yuan, T., Bian, H., Remer, L. A., Prospero, J. M., ... & Zhang, Z. (2015). The fertilizing role of African dust in the Amazon rainforest: A first multiyear assessment based on data from Cloud-Aerosol Lidar and Infrared Pathfinder Satellite Observations. *Geophysical Research Letters*, 42(6), 1984-1991.

Yu, Y., Notaro, M., Kalashnikova, O. V., & Garay, M. J. (2016). Climatology of summer Shamal wind in the Middle East. *Journal of Geophysical Research: Atmospheres*, 121(1), 289-305.

**Figures:**

**SW Monsoon (June to August)**

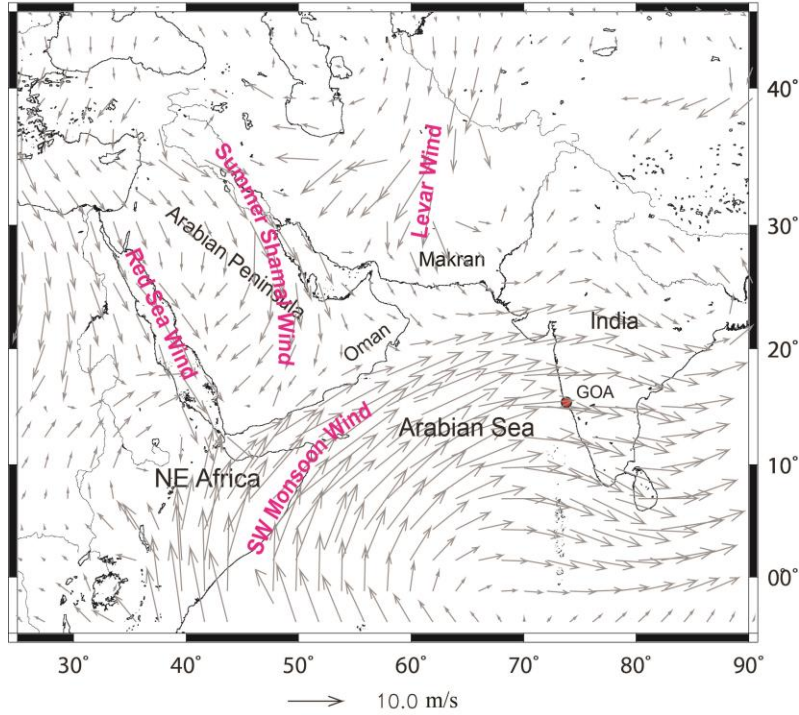


**Fig. 1:** Map showing the sampling site at Goa (Red circle), as well as the possible sources of mineral dust to the Arabian Sea (Black fonts). Major prevailing wind system during the SW monsoon season is highlighted in magenta fonts (climatology of average wind observed during June to August months ).

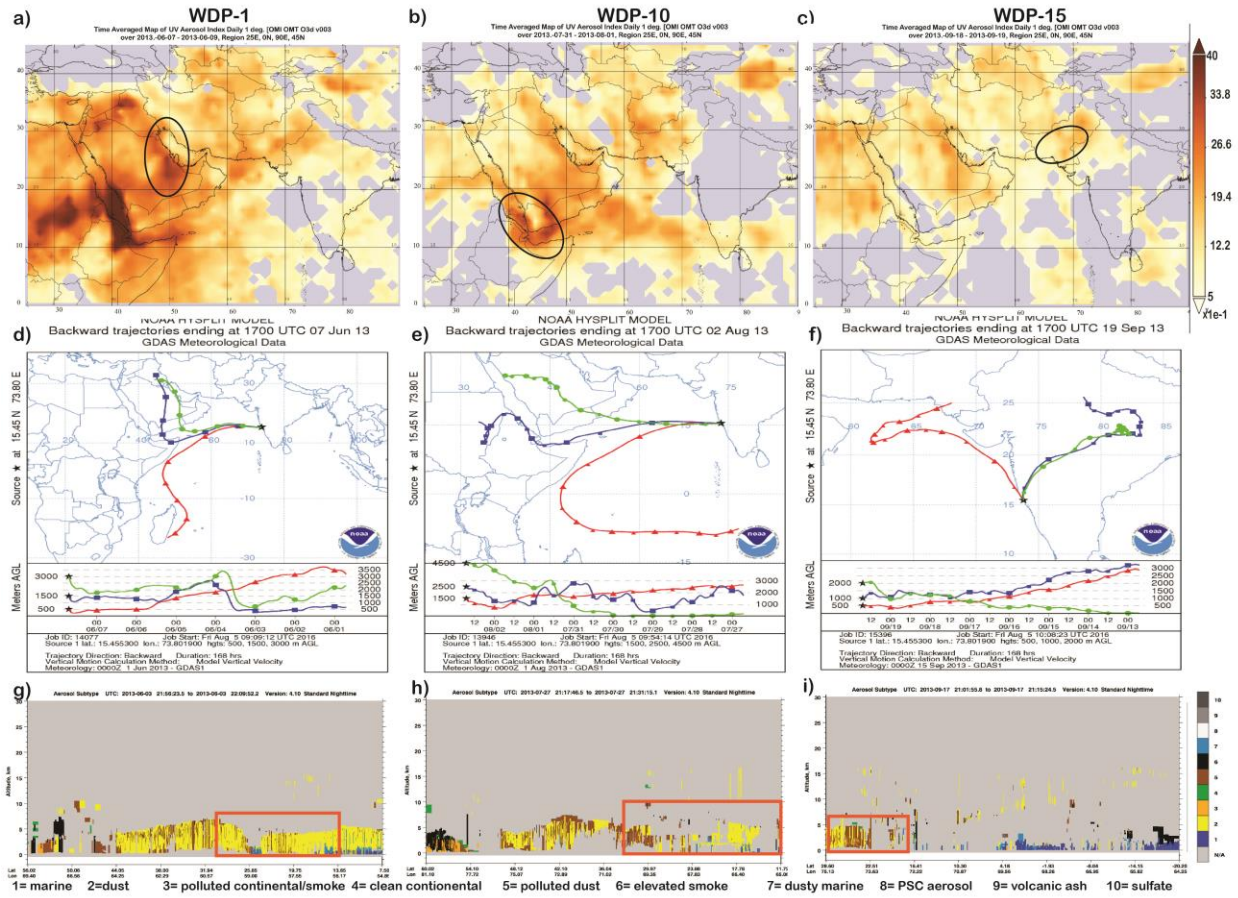


**Fig. 2:** Map showing average UV-aerosol index over source region during the sampling period for WDP samples (a) WDP-1 (b) WDP-10 and (c) WDP-15 collected at beginning, mid and end of the SW monsoon respectively. Air mass back trajectory for 7 days from the sample collection day (d), (e) and (f) shows that the air mass at different altitudes are originating from different source regions. In (d and e) the trajectory at 500 m represents the SW monsoon winds which travels at lower altitudes (500-1500m), whereas the trajectories of higher altitude (>1500m) follows the Shamal wind pathways. At the end of the monsoon (f) the wind trajectories are mainly originates from the SW Asian region showing the change in the dust source. CALIPSO pass available two days before the sampling are shown in (g) WDP-1, (h) WDP-10 and (i) WDP-15, which shows the presence of dust (marked in the orange box, yellow color ‘note no.3 in profile legend’)over the Arabian sea region.



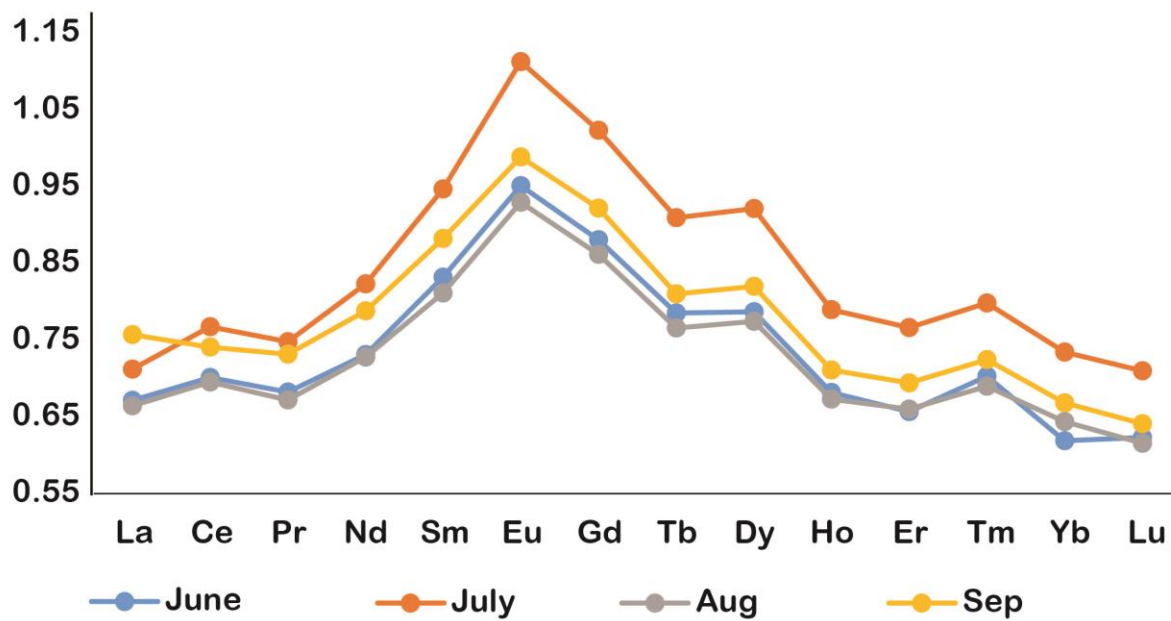


**Fig. 3:** The PAAS normalized REEs pattern of monthly averaged value for the wet deposition particulate samples collected during the SW Monsoon period of 2013.

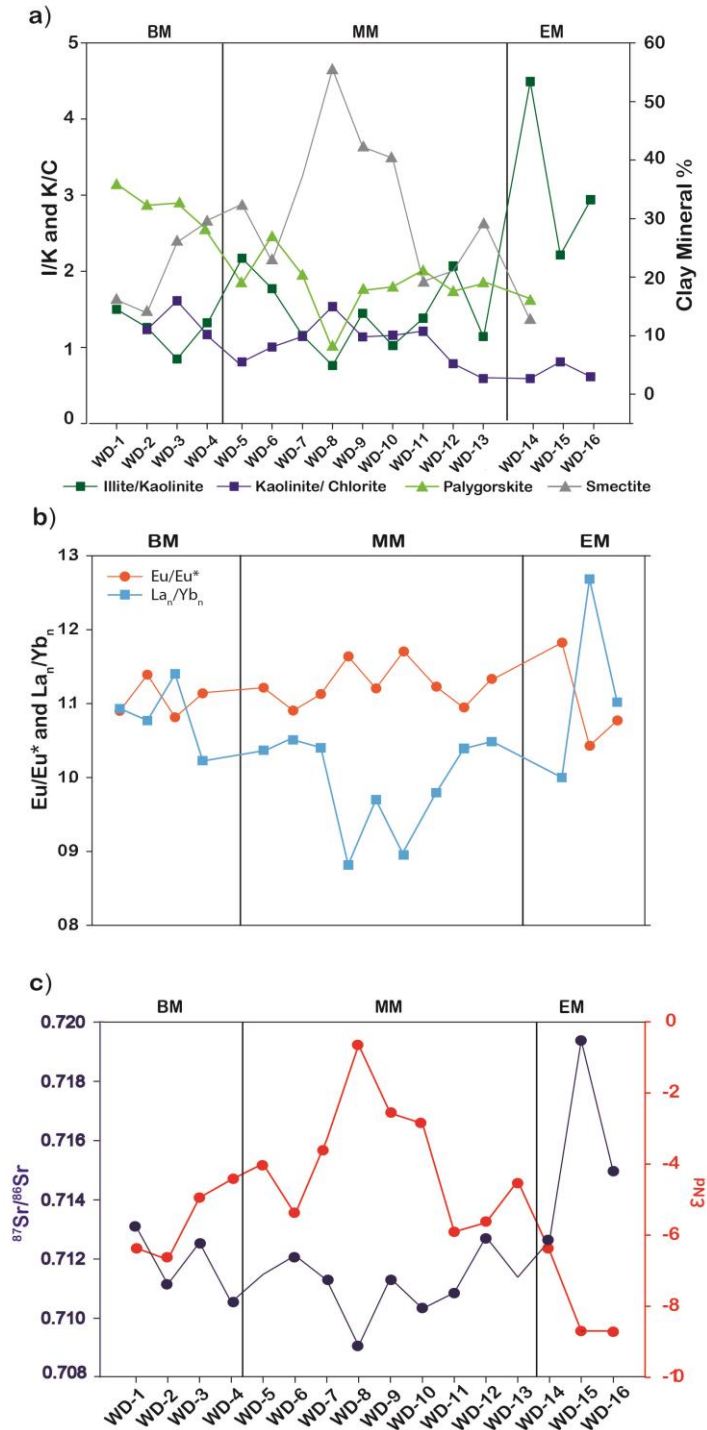


**Fig. 4:** Temporal variation in (a) abundance of palygorskite and smectite as well as illite/kaolinite and kaolinite/chlorite ratio (b) Eu/Eu\* anomaly and La<sub>n</sub>/Yb<sub>n</sub> (c) <sup>87</sup>Sr/<sup>86</sup>Sr and ε<sub>Nd</sub> for the samples collected during the SW monsoon period of 2013 at our sampling location in Goa.

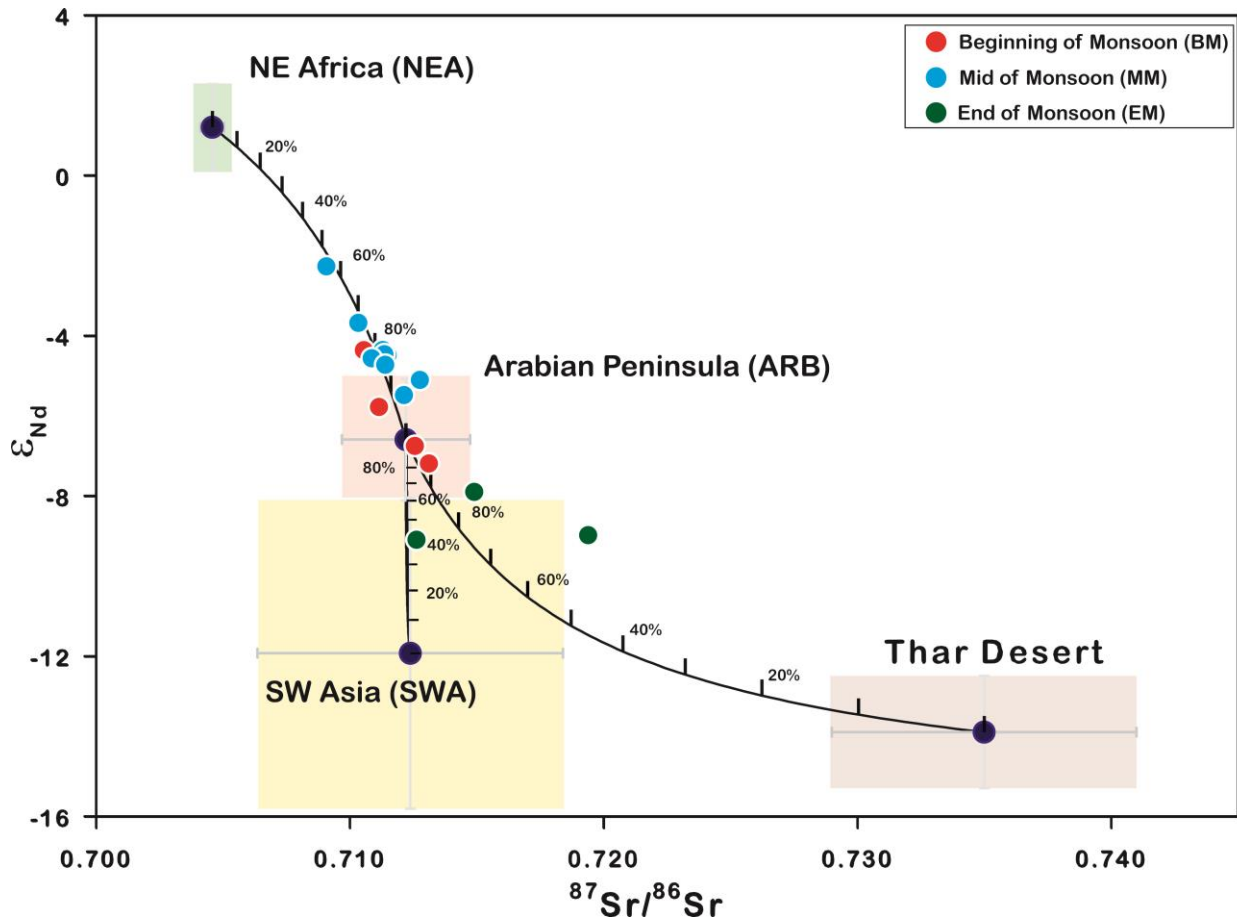


**Fig. 5:** Nd vs. Sr isotopic compositions of the WDP samples plotted along with potential source region isotopic fields inferred from the literature data (see text and Table-3 for detail). Mixing line between ARB and NEA, SWA, Thar Desert are also shown. The ticks on each mixing line correspond to relative contribution of Arabian Peninsula end-member to the mixture.

**Tables:**

**Table 1:** Sample name, date of collection,  $^{87}\text{Sr}/^{86}\text{Sr}$ ,  $^{143}\text{Nd}/^{144}\text{Nd}$  and  $\epsilon_{\text{Nd}}$  values, as well as relative percentages (%) of smectite (S), palygorskite (P), illite (I), chlorite (C) and kaolinite (K)).

\*ND: not detected

Sample ID	Date of collection	$^{87}\text{Sr}/^{86}\text{Sr}$	$\pm 2\sigma$	$^{143}\text{Nd}/^{144}\text{Nd}$	$\pm 2\sigma$	$\epsilon_{\text{Nd}}$	S	P	I	K	C
WDP-1	7-10 June 2013	0.713105	13	0.512270	6	-7.2	16	37	28	19	ND*
WDP-2	11-12 June 2013	0.711142	11	0.512342	5	-5.8	15	34	21	17	13
WDP-3	18-19 June 2013	0.712552	16	0.512293	6	-6.7	27	33	14	16	10
WDP-4	25-26 June 2013	0.710539	10	0.512415	5	-4.4	30	29	17	13	11
WDP-5	29-30 June 2013	0.711477	17	0.512409	5	-4.5	33	19	23	11	13
WDP-6	3-4 July 2013	0.712120	14	0.512358	5	-5.5	23	28	23	13	13
WDP-7	12-13 July 2013	0.711285	18	0.512415	5	-4.3	38	21	16	13	12
WDP-8	18-19 July 2013	0.709067	14	0.512522	6	-2.3	56	8	11	15	10
WDP-9	23-24 July 2013	0.711352	12	0.512410	5	-4.5	43	18	17	12	10
WDP-10	31 July-1 Aug 2013	0.710323	11	0.512450	9	-3.7	42	19	14	13	11
WDP-11	6-7 Aug 2013	0.710855	16	0.512405	7	-4.6	20	22	25	18	15
WDP-12	12-13 Aug 2013	0.712749	17	0.512377	9	-5.1	22	18	29	14	18
WDP-13	17-18 Aug 2013	0.711383	2	0.512396	8	-4.7	30	20	15	13	22
WDP-14	10-11 Sep 2013	0.712616	9	0.512172	12	-9.1	16	13	44	10	17
WDP-15	19-20 Sep 2013	0.719377	15	0.512178	6	-9.0	ND	ND	50	22	28
WDP-16	28-30 Sep 2013	0.714931	12	0.512234	6	-7.9	ND	ND	53	18	29

**Table 2:** The concentrations of major elements and REEs of the wet deposited dust samples collected during the SW monsoon of 2013.

Sample name	WDP-1	WDP-2	WDP-3	WDP-4	WDP-5	WDP-6	WDP-7	WDP-8	WDP-9	WDP-10	WDP-11	WDP-12	WDP-13	WDP-14	WDP-15	WDP-16
%																
<b>Al</b>	6.0	3.9	5.8	6.3	6.6	7.4	7.5	6.5	5.5	6.1	5.6	4.1	6.2	5.1	7.5	5.9
<b>Fe</b>	4.2	3.8	4.2	5.0	5.0	5.2	5.2	5.1	4.0	4.9	4.2	3.3	4.1	5.5	4.9	4.0
<b>Ca</b>	0.5	5.4	0.6	1.7	1.1	0.9	1.0	0.9	0.7	2.0	1.0	0.4	0.5	0.3	0.7	0.8
<b>Mg</b>	2.7	3.2	2.5	3.1	2.7	3.0	2.7	2.0	2.0	3.0	2.2	1.8	2.0	1.4	2.3	2.5
<b>Ti</b>	0.4	0.4	0.4	0.6	0.5	0.6	0.6	0.5	0.5	0.5	0.5	0.3	0.5	0.5	0.5	0.4
ppm																
<b>La</b>	28.2	21.6	24.2	24.8	27.8	30.9	31.3	25.3	24.5	23.3	24.7	24.4	25.1	24.6	37.1	24.7
<b>Ce</b>	63.4	47.3	53.0	52.9	61.9	67.8	71.0	57.4	56.4	54.3	58.0	51.7	54.2	52.2	72.9	52.8
<b>Pr</b>	6.6	5.3	5.6	6.0	6.8	7.4	7.5	6.4	5.9	6.1	6.0	5.7	5.9	5.8	7.9	5.8
<b>Nd</b>	25.3	20.7	21.5	23.2	26.6	28.8	28.8	26.0	23.6	24.5	23.9	22.0	23.0	23.1	30.3	22.2
<b>Sm</b>	4.9	4.1	4.3	4.7	5.3	5.6	5.7	5.4	4.8	5.0	4.7	4.2	4.5	4.5	5.9	4.4
<b>Eu</b>	1.1	1.0	0.9	1.1	1.2	1.2	1.3	1.3	1.1	1.2	1.1	1.0	1.0	1.1	1.2	0.9
<b>Gd</b>	4.4	3.7	3.7	4.3	4.7	5.0	5.2	5.0	4.3	4.5	4.3	3.9	3.9	4.1	5.1	3.9
<b>Tb</b>	0.6	0.5	0.5	0.6	0.7	0.7	0.7	0.7	0.6	0.7	0.6	0.6	0.6	0.6	0.7	0.5
<b>Dy</b>	3.7	3.1	3.1	3.6	4.0	4.2	4.4	4.2	3.7	3.8	3.6	3.3	3.3	3.5	4.2	3.2
<b>Ho</b>	0.7	0.6	0.6	0.7	0.8	0.8	0.9	0.8	0.7	0.7	0.7	0.6	0.6	0.7	0.8	0.6
<b>Er</b>	2.0	1.7	1.7	2.0	2.2	2.3	2.4	2.3	2.0	2.1	2.0	1.8	1.9	2.0	2.3	1.8
<b>Tm</b>	0.3	0.2	0.3	0.3	0.3	0.3	0.3	0.3	0.3	0.3	0.3	0.3	0.3	0.3	0.3	0.3
<b>Yb</b>	1.9	1.5	1.6	1.8	2.0	2.2	2.2	2.1	1.9	1.9	1.9	1.7	1.8	1.8	2.2	1.7
<b>Lu</b>	0.3	0.2	0.2	0.3	0.3	0.3	0.3	0.3	0.3	0.3	0.3	0.3	0.3	0.3	0.3	0.2

**Table 3** Sr and Nd isotopic composition and their concentration of the end-members defined as the Thar Desert, the Arabian Peninsula, SW Asia and the NE Africa.

<b>End members</b>	$^{87}\text{Sr}/^{86}\text{Sr}$	<b>St.dev</b>	<b>Sr (ppm)</b>	$\epsilon\text{Nd}$	<b>St.dev</b>	<b>Nd (ppm)</b>	<b>References</b>
Thar Desert	0.7350	0.006	300	-13.9	1.4	35	Tripathi et al. (2004), Ferrat et al. (2011).
Arabian Peninsula	0.7122	0.003	750	-6.6	1.5	20	Kumar et al., (2020); Sirocko (1995)
SW Asia	0.7124	0.006	107	-11.9	3.8	12	Kumar et al., (2020)
NE Africa	0.7046	0.0004	574	1.7	1.1	32	Ayelew et al (2018)